Rare Metal Materials and Engineering
Volume 51, Issue 6, June 2022
Available online at www.rmme.ac.cn

Science Press

Cite this article as: Yang Xiaoling, Wang Ying, Peng Lin, et al. Influence of Different Cooling Mediums on $\beta\rightarrow\alpha$ Phase Transformation Microstructure and Texture in Commercially Pure Ti[J]. Rare Metal Materials and Engineering, 2022, 51(06): 1957-1963.

ARTICLE

Influence of Different Cooling Mediums on $\beta\rightarrow\alpha$ Phase Transformation Microstructure and Texture in Commercially Pure Ti

Yang Xiaoling[1], Wang Ying[2], Peng Lin[2], Li Jun[2], Luan Baifeng[1]

[1] International Joint Laboratory for Light Alloys (Ministry of Education), College of Materials Science and Engineering, Chongqing University, Chongqing 400044, China; [2] Panzhihua Iron and Steel Research Institute, Chengdu 610031, China

Abstract: The effect of cooling medium on microstructure evolution, variant selection and texture inheritance along with mechanical properties in a recrystallized commercially pure Ti sheet after β-solution treatment was investigated by combined use of optical microscopy (OM), electron channeling contrast (ECC) imaging, electron backscatter diffraction (EBSD) techniques, transmission electron microscopy (TEM) and micro-hardness test. It is found that with the decrease of cooling rate, fine needle-like α' martensite (in water and liquid nitrogen), Widmanstätten (in air), and coarse-grain microstructures (in furnace) are observed in turn. Additionally, the faster cooling rate results in a finer transformed structure accompanied with an attendant higher hardness value. Analyses for crystallographic orientations reveal that the Burgers orientation relationship (BOR) is strictly obeyed during the $\beta\rightarrow\alpha$ cooling except for the β-furnace-cooled specimen with appearance of other misorientations disobeying the BOR. As for texture characteristics, firstly, the texture distribution is largely scattered compared with the initial one and new orientation components of <0001>//TD and <11$\bar{2}$0>//ND appear upon the water and liquid nitrogen quenching. Secondly, the texture inheritance phenomenon occurs in furnace cooling condition because of stronger variant selection, then leading to a stronger transformation texture. Results suggest that raising cooling rates can be more feasible to weaken the transformation texture by suppressing the variant selection.

Key words: commercially pure Ti; microstructure evolution; variant selection; texture inheritance

Ti and its alloys have important applications in aerospace, marine, automotive, biomedical and energy industries because of their high specific strength, excellent corrosion resistance and high biocompatibility[1-3]. Compared with traditional fabrication technologies, β-solution treatment is one of the most effective ways for the tailors of comprehensive properties by modifying the heat treatment parameters such as solution temperature, holding time and cooling rate. Among the above heat treatment variables, cooling rate is generally regarded as a key factor that effectively determines the $\beta\rightarrow\alpha$ phase transformation mechanism along with microstructures, which has already attracted a lot of attention[4-6].

It is well known that titanium has close packed hexagonal (hcp) crystal structure at low temperatures and body centered cubic (bcc) structure at high temperatures. Generally, the β parent phase and α product phase during $\beta\rightarrow\alpha$ phase transformation are oriented according to the Burgers orientation relationship (BOR)[7]: $\{110\}_{\beta}//\{0001\}_{\alpha}$ and $<111>_{\beta}//<11\bar{2}0>_{\alpha}$, which have been confirmed in many Ti alloys for both diffusional and martensitic transformations[8-11]. Based on BOR and the crystal symmetry, theoretically, one prior β grain can transform into twelve variants with equal probability during the $\beta\rightarrow\alpha$ phase transformation. Accordingly, a relatively randomized α texture can be obtained[12,13]. However, due to the appearance of variant selection (certain variants are formed more frequently than others), a similar or even stronger transformed α texture is often obtained in practice. For example, Lonardelli et al[14] studied the $\beta\rightarrow\alpha$ transformation of cold-rolled commercially pure Ti sheet and revealed that a strong selection of α variants occurs probably to minimize the grain boundary energy. In another study, Romero[15] et al found that hardly any variant selection was

Received date: June 12, 2021
Foundation item: National Natural Science Foundation of China (51421001); Fundamental Research Funds for the Central Universities (2020CDJDPT001)
Corresponding author: Luan Baifeng, Ph. D., Professor, International Joint Laboratory for Light Alloys (Ministry of Education), College of Materials Science and Engineering, Chongqing University, Chongqing 400044, P. R. China, Tel: 0086-23-65106067, E-mail:bfluan@cqu.edu.cn

observed during $\alpha \rightarrow \beta$ phase transformation. But when the material was rapidly cooled back above the β-transus, the α texture exhibits moderate variant selection. They also reported that incomplete transformations (i. e. the β transus was not completely exceeded) exhibited perfect texture memory probably caused by the insufficient β grain growth, favoring the nucleation of α variant in special β grain boundaries. Beladi et al[16] suggested that the small phase transformation driving force at a high transformation temperature results in the selection of a specific variant to nucleate preferentially at a given β grain boundary during slow cooling. While with an increase of cooling rate, the differences in the activation energies for the nucleation of different α variants are reduced, promoting different variant formation to self-accommodate the transformation strain. Similarly, Dai et al[17] have also found that slow cooling facilitates preferable nucleation of α phases at β boundaries and strengthens variant selection, leading to greatly intensified transformation textures; rapid cooling weakens the transformation texture due to suppressed variant selection through easier nucleation inside β grains.

In spite of previous extensive studies on the microstructure and texture of Ti during phase transformation, the influence of cooling medium (corresponding to different cooling rates) during $\beta \rightarrow \alpha$ process on both microstructure evolution and variant selection behavior, which result in different phase transformation textures, has rarely been reported in commercially pure titanium. However, the microstructure and texture are the key factors for the high performance of commercially pure titanium stamping products. Therefore, the research of the effects of cooling rates on phase transformation products is helpful to deeply understand the evolution of microstructure and the nature of various mechanical properties during hot deformation and to provide a theoretical basis for the heat treatment regime optimization in Ti sheet and other industrial products.

1 Experiment

The as-received material employed in the present work was a full-recrystallized commercially pure Ti (TA1) sheet with an $\alpha+\beta$ dual-phase region in the range of 875~912 ℃ determined by differential scanning calorimeter. The chemical composition (wt%) of the alloy was: 0.02 Fe, 0.039 O, 0.003 N, 0.013 C, 0.001 H and Ti balanced. Rectangular specimens with dimensions of 7, 5 and 0.6 mm were cut from the as-received material, corresponding to their rolling direction (RD), transverse direction (TD) and normal direction (ND), respectively. The specimens were sealed into quartz tubes under vacuum to avoid oxidation and then treated at 1050 ℃ for 40 min. Subsequently, the sealed specimens were cooled down to room temperature in water, liquid nitrogen, air and furnace, denoted as WC, NC, AC and FC, respectively.

In this study, all the observations were performed on RD-TD plane of these specimens and the surfaces to be examined were mechanically ground and then electro-polished at 30 V and −30 ℃. Macro-morphology observation and microstructural characterization were conducted with optical metallography (OM) and electron channeling contrast (ECC) imaging technique, respectively. Crystallographic orientation and texture of samples were determined and analyzed by FEI Nova 400 scanning electron microscope (SEM) equipped with an Oxford EBSD system. TEM observations were carried out on FEI Tecnai G^2 F20 equipment at an accelerating voltage of 200 kV. In addition, hardness measurements were carried out on a Vickers indentation tester at an indenting load of 300 g for 15 s. The mean hardness and its standard deviation were calculated through 30 measurements made in arbitrary positions, roughly-evenly distributed.

2 Results and Discussion

2.1 Microstructure characterization

Microstructures of all specimens measured by OM are displayed in Fig. 1. The initial microstructure (Fig. 1a) is populated by equiaxed α grains with relatively uniform size, which indicates that complete recrystallization occurs. By the linear intercept method, an average size of recrystallized grains is ~15 μm. The images of β-solution treated specimens with different cooling rates are shown in Fig.1b~1e. It can be clearly seen that the original β grain boundaries (marked by white dash line in Fig. 1b~1d) are retained when cooled in water, liquid nitrogen and air. Based on these residual β grain boundaries, the prior β grain size is measured to be 360 μm on average. As shown in Fig.1b and 1c, except for the nucleation inside the prior β grains, α' laths also grow from the β grain boundary toward inside. However, no α' phase continuously nucleates along the grain boundary to form α layer. This can be ascribed to the fact that the high β-cooling rates will lead to a large undercooling and the fast kinetics of transformation, which allows for abundant nucleation sites for α' laths. Fig.1d shows the microstructure of the air-cooled sample, from which net-like grain boundary α films (as indicated by red dash line) decorate the prior β grain boundaries and large colonies of α lamellar (marked by green dash line) within β grains can be easily identified. A possible explanation accounting for this phenomenon in the air-cooled specimen may be the existence of high energy β grain boundaries and the moderate cooling rate, which provide sufficient time for α phases to firstly nucleate and grow in preferred orientation along the prior β grain boundary and subsequently within the grain interior, resulting in the formation of α films with specific orientation and α colonies. Inversely, original β grain boundaries are no longer observed but completely replaced by coarse grains in the specimen cooled in furnace (Fig.1e).

Due to the limited metallographic resolution, the microstructures of specimens after $\beta \rightarrow \alpha$ transformation at various cooling rates are characterized in detail by ECC in Fig.2. It can be seen from Fig.2a that most of the grains in WC specimen are composed of the fine acicular martensite, which geometrically combine with each other to form a triangular shape configuration (as indicated by the dashed triangle). It has been reported that specific three-variant clustering takes place during the martensitic transformation to self-

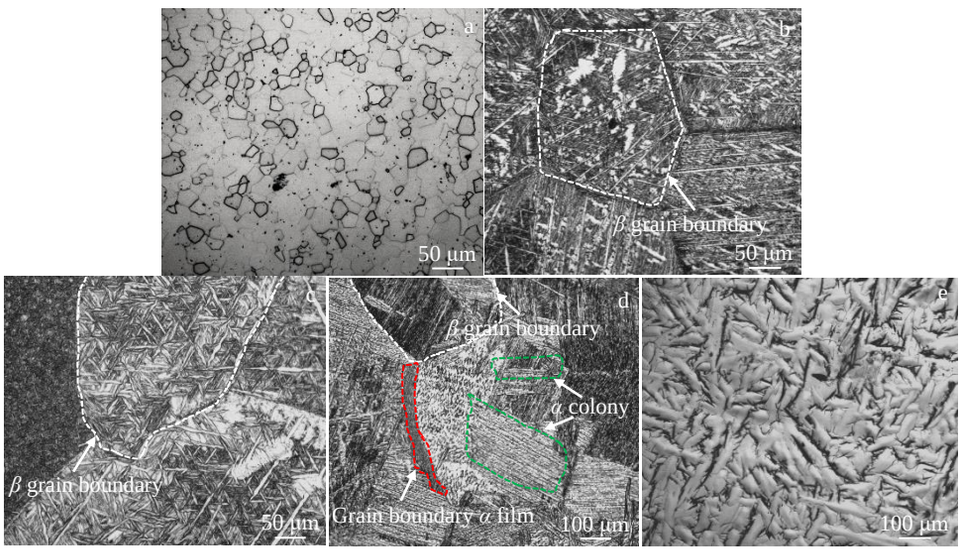

Fig.1 Optical micrographs of specimens: (a) as-received, (b) WC, (c) NC, (d) AC and (e) FC

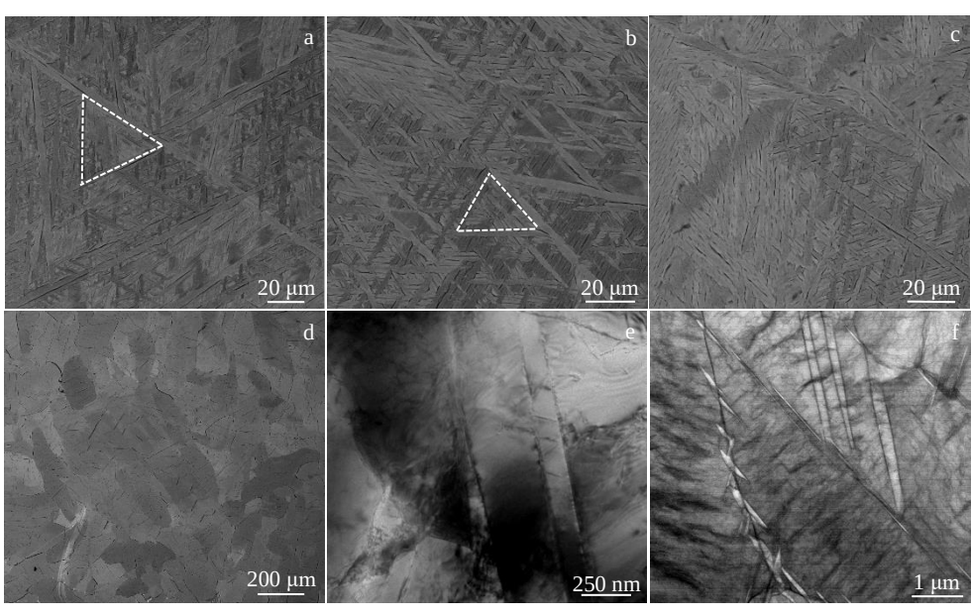

Fig.2 ECC images of specimens after WC (a), NC (b), AC (c) and FC (d) and TEM bright-field images of specimens after WC (e) and NC (f)

accommodate the shape strains[18,19]. As shown in Fig. 2b, liquid nitrogen cooling also results in a similar transformed microstructure. Fig. 2e and 2f show the TEM bright-field images of WC and NC specimens, from which a high density of dislocations can be observed within the α' martensite plates. In fact, this typical α' martensite microstructure has been commonly reported in many Ti alloys[20-22].

As illustrated in Fig.2c, the microstructure of AC specimen corresponds to the so-called Widmanstätten including both basketweave structure inside β grain and parallel plates within intersected α colonies. It is reported that those colonies compete with the neighboring colonies and partially impinge each other when growing from the β grain boundaries toward the interior of the grain[23]. Such is also the case in the present investigation. From Fig. 2d, one can clearly see that the microstructure of the furnace-cooled specimen is composed of coarse grains, which should be related to limited nucleation rates because of small undercoolings induced by the slow cooling. Moreover, both the Widmanstätten and coarse-grain structures have no specific variant arrangement resulting from the decreased transformation strain during the diffusive transformation, leading to a more random distribution of intervariant boundaries[24].

2.2 Microhardness testing

The mean α-lath width (the mean grain size in the as-received specimen) and hardness values of specimens as a function of cooling rate are plotted in Fig. 3. Obviously, the faster the cooling rate, the higher the microhardness. A possible explanation accounting for this can be analyzed in light of the above microstructural characteristics. With respect

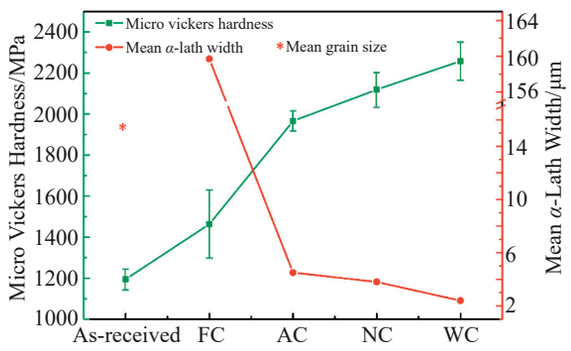

Fig.3 Mean α-lath width and micro Vickers hardness variation under different β-cooling conditions in TA1

to the WC specimen, the finest α lath (~2.4 μm) possesses the densest grain boundaries compared with all the specimens investigated, which can effectively act as the dislocation barriers, and thus produce a maximum hardness of 2250 MPa. Whereas for the NC specimen, the resistance of grain boundaries to dislocation movements will be weakened with a coarser α lath (~3.8 μm). Consequently, a comparatively low hardness of 2110 MPa is obtained. The AC and FC specimens, which own larger widths of α product phase (~4.5 μm and ~159.7 μm, respectively), show further lower hardness of 1960 and 1460 MPa, respectively. At the same time, the hardness of specimens after annealing at β phase field is always higher than that of the as-received material regardless of cooling rates. This can possibly be attributed to the formation of many elongated fine laths, which can impede dislocation migration as grain boundary does, leading to the increased hardness[20].

2.3 Orientation analysis

Fig. 4 gives EBSD characterization results of the as-received specimen. According to Fig. 4a, we note that <0001> directions of most grains are aligned toward the ND of the sheet. Also noticed from Fig. 4b, its misorientation angle distribution histogram resembles a random case except a slight concentration around 30° and 70°.

Local crystallographic orientations within one prior β grain of WC specimen is presented in Fig. 5. It can be seen from Fig. 5a that all the 12 orientations are definitely observed and marked by consecutive numbers, which correspond to 12 α variants according to the BOR[7]. Also, the BOR predicts that all possible intervariant boundaries formed by two different α variants adjoining in one prior β grain can be described by only five independent misorientation angles and axis, namely 10.5°/<0001>, 60°/<11$\bar{2}$0>, 60.8°/<12$\bar{3}$1>, 63.3°/<44$\bar{8}$3> and 90°/<12$\bar{3}$0>[25] (marked by n_1, n_2, n_3, n_4, n_5, respectively).

Fig. 5b shows more crystallographic characteristics of these variants revealed by {0001} and {11$\bar{2}$0} pole figures. According to the {0001} pole figure, all the 12 α variants can be separated into six pairs. Each pair of variants, such as variants 1 and 2, have their basal planes parallel to each other, while the <11$\bar{2}$0> axes of any two variants belonging to one pair slightly deviate from each other by about 10°, corresponding well to the first Burgers misorientation (10.5°/<0001>). In the {11$\bar{2}$0} pole figure, the 12 orientations can also be classified as four groups, and each group includes three orientations (like those numbered by 1, 4 and 5) sharing one <11$\bar{2}$0> direction. It is also noted that there is about 60° between their c-axes. The orientation relationship between these variants thus can be expressed as ~60°/<11$\bar{2}$0>, which is coincident with the second Burgers misorientation. The situation is the same for variants 2, 10 and 11, variants 3, 7 and 12, and variants 6, 8 and 9. The above orientation relationships can be better visualized from the three-dimensional crystal orientations in {0001} pole figure.

As shown in Fig. 5c, there are three evident peaks around 10°, 60° and 90° in the misorientation angle distribution map of WC sample. A rotation-axis analysis for its peak near 60° reveals three preferred rotation axes of <11$\bar{2}$0>, <12$\bar{3}$1> and <44$\bar{8}$3>, suggesting that this peak is superposition of the second, the third and the fourth Burgers misorientations. Accordingly, the peaks near 10° and 90° reveal the first and the fifth Burgers misorientations, respectively.

Such results thus suggest that the classical BOR is well followed in the WC specimen. By further analyses, the same conclusions can be obtained in the NC and AC specimens (not illustrated here due to space constraints).

In order to better understand the effect of cooling mediums on variant selection, the occurrence frequencies (in area

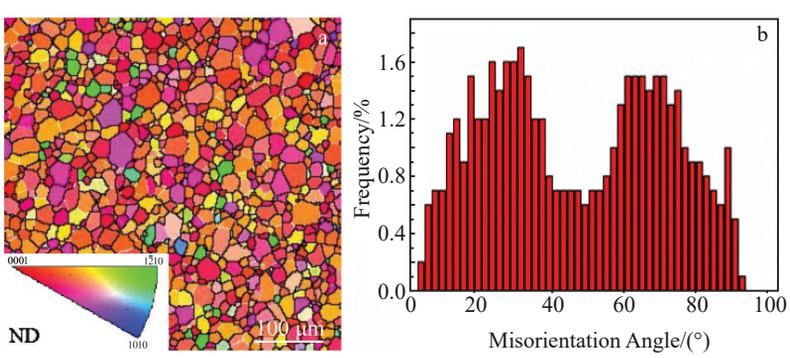

Fig.4 EBSD IPF map (a) and corresponding misorientation angle distribution (b) of the as-received specimen

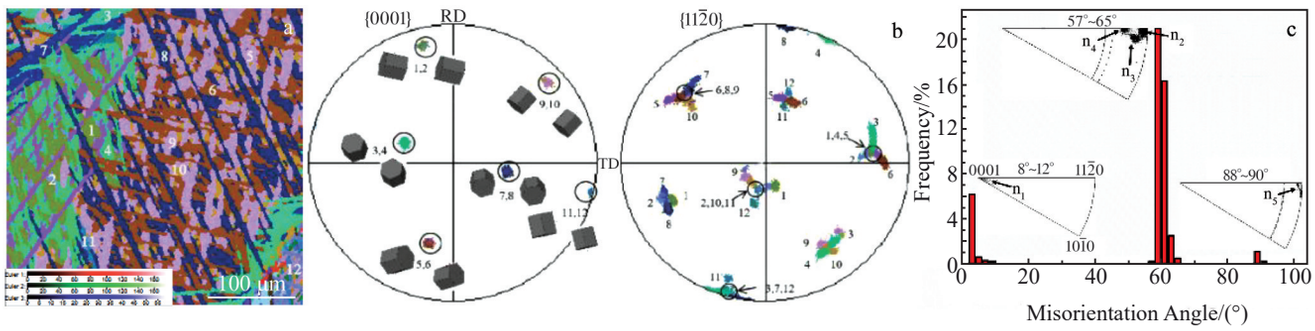

Fig.5 EBSD orientation imaging map of WC specimen reconstructed from all Euler angles within one prior β grain (different colors represent various crystallographic orientations of 12 α variants indicated by consecutive numbers) (a); {0001} and {11$\bar{2}$0} pole figures corresponding to Fig.5a (b) and misorientation angle histogram and rotation axis distribution (c)

Table 1 Area fraction of each α variant within one prior β grain under the condition of WC, NC, and AC (%)

α variant	V1	V2	V3	V4	V5	V6	V7	V8	V9	V10	V11	V12
WC	4.8	9.1	5.3	21.5	7.1	18.1	18.9	4.0	3.3	0.2	6.6	1.1
NC	11.2	5.2	5.7	5.6	13.1	2.9	10.8	9.7	7.2	4.7	14.6	9.3
AC	2.4	15.7	9.3	4.0	6.1	1.9	6.1	15.2	1.7	13.3	1.5	22.8

fraction) of each α variant within one prior β grain obtained from the local EBSD map are estimated and presented in Table 1, in which all of them are more or less away from the ideal proportion expected from the BOR[26]. A possible explanation is that there is existence of variants preferential nucleation and growth during the $\beta \rightarrow \alpha$ phase transformation. It has been reported that cooling rate can alter the dominant variant selection mechanism from three-variant clustering at high cooling rate, which results in a distinct difference in the exact volume fraction of variants[24,27].

Fig.6a and 6b illustrate EBSD orientation imaging map and pole figures of the FC specimen, where strong variant selection has occurred so that very limited numbers among all the 12 α variants are detected. Similarly, Gey et al[28] investigated the orientation distribution of α_s laths in a near-α titanium and found only a few variants produced through a slow cooling rate. Humbert et al[29] pointed out that only those variants with the strain elastic energy lower than a given threshold can appear. Hence variant numbers presented in the FC specimen will be fewer. It can be seen from Fig. 6c that even though there are three sharp peaks near 10°, 60° and 90°, other misorientations that do not meet the expectations of BOR also can be clearly seen. This indicates that the obedience of the BOR is much less strict during furnace cooling.

2.4 Texture measurement

Fig. 7 displays the texture evolution of specimens before and after $\beta \rightarrow \alpha$ transformation with different cooling rates, which is derived from EBSD datasets in the same scanning area (including thousands of grains) to insure reliable textural comparisons. As shown in Fig. 7a, the as-received specimen presents a typical split bimodal basal texture. After β heat treatment, however, changes are noted for texture characteristics. From Fig. 7b~7e, the intensity of bimodal basal texture gradually decreases with the occurrence of several scattered new orientations such as <0001>//TD and <11$\bar{2}$0>// ND in WC and NC samples and then conversely increases due to their disappearance under the condition of air and furnace

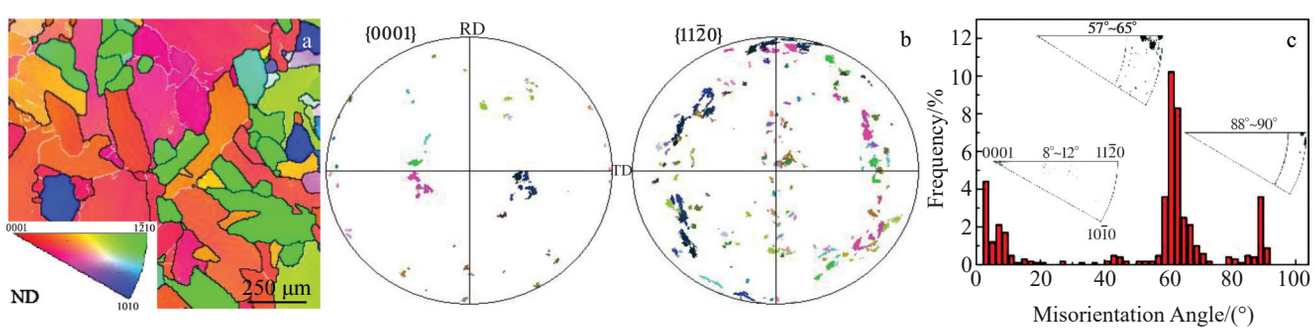

Fig.6 EBSD orientation imaging map of FC specimen (a), {0001} and {11$\bar{2}$0} pole figures corresponding to Fig.6a (b), and misorientation angle histogram and rotation axis distribution (c)

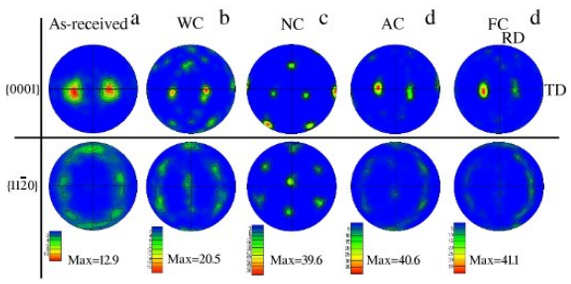

Fig.7 {0001} and {11$\bar{2}$0} pole figures of as-received (a), WC (b), NC (c), AC (d) and FC (e) specimens (corresponding to an EBSD scanning area of 2 mm×1.5 mm)

cooling. More importantly, the texture characteristics of the furnace-cooled specimen are almost the same as those of as-received specimen. This phenomenon may be associated with the texture inheritance caused by variant selection[30-32].

At the same time, it is also worth noting that the overall peak intensity of transformation texture in rapid water-quenched specimen is considerably weaker than that in slower cooling cases, which is consistent with the previous reports[17,33]. It can be reasonably concluded that raising cooling rate may be a feasible way to weaken the transformation texture. The rapid cooling is able to induce a large undercooling, which allows more α variants with scattered orientations to be produced, thus weakening the transformation texture[34]. Nevertheless, at slower cooling rate, prior β grain boundaries or the grain boundary α layers can act as preferred nucleation sites of certain variants and consequently variant selection occurs, leading to textural strengthening[35,36]. In summary, above results of the texture measurement imply that the variation of cooling rate can not only change the texture distribution but also effectively modify the intensity of inherited texture in fully β-treated CP-Ti.

3 Conclusions

1) Three distinct morphologies can be obtained after specimen cooling in different mediums. That is, rapid cooling in water and liquid nitrogen leads to fine needle-shaped α' martensite, while slower cooling produces Widmanstätten α phase (air cooling) or coarse-grain microstructures (furnace cooling). Moreover, the size of α product phase increases with the decrease of cooling rate during $\beta \rightarrow \alpha$ transformation, eventually leading to the decreased micro-hardness.

2) All 12 potential α variants together in one prior β grain are observed and the classical BOR is strictly followed under the condition of water, liquid nitrogen and air cooling. For the furnace cooled specimen, however, not only the less strict obedience of BOR but also few out of 12 variants are observed owing to strong variant selection.

3) Textural intensity and distribution after β zone solution can be well controlled by modifying cooling rate. More specifically, rapid cooling in water leads to considerably weakened and scattered transformation texture; while slower cooling produces more intensified texture. Besides, remarkable texture inheritance phenomenon is more prone to occur after the very slow $\beta \rightarrow \alpha$ cooling in the TA1 sheet.

References

1 Boyer R R. *Materials Science and Engineering A*[J], 1996, 213(1): 103
2 Poondla N, Srivatsan T S, Patnaik A *et al. Journal of Alloys and Compounds*[J], 2009, 486(1): 162
3 Nasiri-Abarbekoh H, Ekrami A, Ziaei-Moayyed A A. *Materials and Design*[J], 2012, 37: 223
4 Zhou W, Zhao Y Q, Xin S W *et al. Rare Metal Materials and Engineering*[J], 2020, 49(7): 2314
5 Gil F J, Manero J M, Ginebra M P *et al. Materials Science and Engineering A*[J], 2003, 349(1): 150
6 Oh M S, Lee J Y, Park J K. *Metallurgical and Materials Transaction A*[J], 2004, 35(10): 3071
7 Burgers W G. *Physica*[J], 1934, 1(7): 561
8 Sun F, Liu X H, Li J S *et al. Rare Metal Materials and Engineering*[J], 2020, 49(1): 68
9 Bhattacharyya D, Viswanathan G B, Fraser H L. *Acta Materialia* [J], 2007, 55(20): 6765
10 Shi R, Dixit V, Fraser H L *et al. Acta Materialia*[J], 2014, 75: 156
11 Stanford N, Bate P S. *Acta Materialia*[J], 2004, 52(17): 5215
12 Sridharan N, Chaudhary A, Nandwana P *et al. JOM*[J], 2016, 68(3): 772
13 Wang Y Z, Ma N, Chen Q *et al. JOM*[J], 2005, 57(9): 32
14 Lonardelli I, Gey N, Wenk H R *et al. Acta Materialia*[J], 2007, 55(17): 5718
15 Romero J, Preuss M, Quinta da Fonseca J *et al. Acta Materialia* [J], 2009, 57(18): 5501
16 Beladi H, Chao Q, Rohrer G S. *Acta Materialia*[J], 2014, 80: 478
17 Dai J H, Xia J Y, Chai L J *et al. Journal of Materials Science*[J], 2020, 55(19): 8346
18 Balachandran S, Kashiwar A, Choudhury A *et al. Acta Materialia* [J], 2016, 106: 374
19 Wang S C, Aindow M, Starink M J. *Acta Materialia*[J], 2003, 51(9): 2485
20 Kao Y L, Tu G C, Huang C A *et al. Materials Science and Engineering A*[J], 2005, 398(1): 93
21 Sun F, Li J S, Kou H C *et al. Rare Metal Materials and Engineering*[J], 2015, 44(4): 848
22 Kim S K, Park J K. *Metallurgical and Materials Transactions A* [J], 2002, 33(4): 1051
23 Wu C, Zhao Y Q, Huang S X *et al. Journal of Alloys and Compounds*[J], 2020, 841: 155 728
24 Farabi E, Tari V, Hodgson P D *et al. Materials Characterization* [J], 2020, 169: 110 640
25 Chai L J, Chen B F, Zhou Z M *et al. Materials Characterization*

[J], 2015, 104: 61
26 Zhao Z B, Wang Q J, Hu Q M *et al. Acta Materialia*[J], 2017, 126: 372
27 Sargent G A, Kinsel K T, Pilchak A L *et al. Metallurgical and Materials Transactions A*[J], 2012, 43(10): 3570
28 Gey N, Bocher P, Uta E *et al. Acta Materialia*[J], 2012, 60(6): 2647
29 Humbert M, Gey N. *Acta Materialia*[J], 2003, 51(16): 4783
30 Wei Z, Yang P, Gu X F *et al. Materials Characterization*[J], 2020, 164: 110 359
31 Obasi G C, Birosca S, Leo Prakash D G *et al. Acta Materialia* [J], 2012, 60(17): 6013
32 Daymond M R, Holt R A, Cai S. *Acta Materialia*[J], 2010, 58(11): 4053
33 Chai L J, Wang T T, Ren Y *et al. Metals and Materials International*[J], 2018, 24(4): 673
34 Chai L J, Xia J Y, Zhi X Y *et al. Materials Chemistry and Physics*[J], 2018, 213: 414
35 Karthikeyan T, Dasgupta A, Khatirkar R *et al. Materials Science and Engineering A*[J], 2010, 528(2): 549
36 Zhao Z, Chen J, Lu X F *et al. Materials Science and Engineering A*[J], 2017, 691:16

冷却介质对商业纯钛$\beta\rightarrow\alpha$相转变组织及织构的影响

杨晓玲[1]，王　莹[2]，彭　琳[2]，李　军[2]，栾佰峰[1]
(1. 重庆大学 材料科学与工程学院 国际轻合金联合实验室(MOE)，重庆 400044)
(2. 攀钢研究院，四川 成都 610031)

摘　要：利用OM、ECC、EBSD、TEM等表征技术和显微硬度实验研究了经β固溶处理的商业纯钛板材在$\beta\rightarrow\alpha$相变过程中不同冷却介质对其组织演变、变体选择、织构遗传及力学性能的影响。结果表明：随着冷却速率的降低，相变组织依次呈细针状α'马氏体（水冷和液氮冷）、Widmanstätten组织（空冷）及粗大晶粒（炉冷），且冷却速率越快，则转变组织越细，进而其硬度值越高。在$\beta\rightarrow\alpha$冷却过程中，只有炉冷条件下由于出现了部分不满足Burgers关系的取向，导致其并不严格遵循Burgers取向关系。与原始组织相比，水冷和液氮冷条件下由于出现新的织构成分（<0001>//TD、<11$\bar{2}$0>//ND），导致其织构分布更分散；炉冷条件下由于发生了强烈变体选择而出现织构遗传现象，导致更强的相变织构。因此可以通过提高冷却速率来抑制变体选择，进而弱化相变织构。

关键词：商业纯钛；组织演变；变体选择；织构遗传

作者简介：杨晓玲，女，1996年生，硕士，重庆大学材料科学与工程学院，重庆 400044，电话：023-65106067，E-mail：1090058007@qq.com